

# Deep Feature Aggregation with Heat Diffusion for Image Retrieval

Shanmin Pang<sup>1</sup> Jin Ma<sup>1</sup> Jianru Xue<sup>1</sup> Jihua Zhu<sup>1</sup> Vicente Ordonez<sup>2</sup>

<sup>1</sup>Xi'an Jiaotong University, <sup>2</sup>University of Virginia

## Abstract

Image-level feature descriptors obtained from convolutional neural networks have shown powerful representation capabilities for image retrieval. In this paper, we present an unsupervised method to aggregate deep convolutional features into compact yet discriminative image vectors by simulating the dynamics of heat diffusion. A distinctive problem in image retrieval is that repetitive or *bursty* features tend to dominate feature representations, leading to less than ideal matches. We show that by considering each deep feature as a heat source, our unsupervised aggregation method is able to avoid over-representation of *bursty* features. We additionally provide a practical solution for the proposed aggregation method, and further show the efficiency of our method in experimental evaluation. Finally, we extensively evaluate the proposed approach with pre-trained and fine-tuned deep networks on common public benchmarks, and show superior performance compared to previous work.

Image retrieval has always been an attractive research topic in the field of computer vision. By allowing users to search similar images from a large database of digital images, it provides a natural and flexible interface for image archiving and browsing. Convolutional Neural Networks (CNNs) have shown remarkable accuracy in tasks such as image classification, and object detection. Recent research has also shown positive results of using CNNs on image retrieval (Babenko and Lempitsky 2015; Kalantidis, Mellina, and Osindero 2016; Hoang et al. 2017). However, unlike image classification approaches which often use global feature vectors produced by fully connected layers, these methods extract local features depicting image patches from the outputs of convolutional layers and aggregate these features into *compact* (a few hundred dimensions) image-level descriptors. Once meaningful and representative image-level descriptors are defined, visually similar images are retrieved by computing similarities between pre-computed database feature representations and query representations.

In this paper we devise a method to avoid over-representing *bursty* features. Inspired by an observation of similar phenomena in textual data, Jegou *et al.* (Jégou, Douze, and Schmid 2009) identified *burstiness* as the phenomenon by which overly repetitive features within an instance tend to dominate the instance feature representation.

In order to alleviate this issue, we propose a feature aggregation approach that emulates the dynamics of heat diffusion. The idea is to model feature maps as a heat system where we weight highly the features leading to low system temperatures. This is because that these features are less connected to other features, and therefore they are more distinctive. The dynamics of the temperature in such system can be estimated using the partial differential equation induced by the heat equation.

Heat diffusion, and more specifically anisotropic diffusion, has been used successfully in various image processing and computer vision tasks. Ranging from the classical work of Perona and Malik (Perona and Malik 1990) to further applications in image smoothing, image regularization, image co-segmentation, and optical flow estimation (Zhang, Zheng, and Cai 2010; Tschumperle and Deriche 2005; Kim et al. 2011; Bruhn, Weickert, and Schnörr 2005). However, to our knowledge, it has not been applied to weight features from the outputs of a deep convolutional neural network. We show that by combining this classical image processing technique with a deep learning model, we are able to obtain significant gains against previous work.

Our contributions can be summarized as follows:

- By greedily considering each deep feature as a heat source and enforcing the temperature of the system be a constant within each heat source, we propose a novel efficient feature weighting approach to reduce the undesirable influence of *bursty* features.
- We provide a practical solution to computing weights for our feature weighting method. Additionally, we conduct extensive quantitative evaluations on commonly used image retrieval benchmarks, and demonstrate substantial performance improvement over existing unsupervised methods for feature aggregation.

## Related Work

Since our deep feature aggregation method is built on heat diffusion, we therefore first review classical diffusion methods for retrieval. Second, we review representative deep learning based image retrieval methods as this paper also aims to address the image retrieval problem with convolutional neural networks.

## Anisotropic Diffusion for Image Retrieval

Anisotropic diffusion is popular in the context of retrieval (Egozi, Keller, and Guterman 2010; Yang, Koknar-Tezel, and Latecki 2009; Donoser and Bischof 2013; Furuya and Ohbuchi 2015; Iscen et al. 2017a). Among them, the approaches (Egozi, Keller, and Guterman 2010; Yang, Koknar-Tezel, and Latecki 2009; Furuya and Ohbuchi 2015) focused on shape retrieval, and performed diffusion on image level. While we address the instance-level retrieval problem, and we carry out heat diffusion on deep convolutional features. Donoser and Bischof (Donoser and Bischof 2013) reviewed a number of diffusion mechanisms for retrieval. They focused on iterative solutions arguing that closed form solutions, when existing, are impractical due to inversion of large matrices. However, we focus on a closed form solution without iteration as in our case the number of features and the number of re-ranking images are small. Recently, Iscen *et. al* (Iscen et al. 2017a) introduced a regional diffusion mechanism on image regions for better measuring similarities between images. Compared with this method, our re-ranking method is much efficient as we re-rank images based on global level image vectors.

Democratic Diffusion Aggregation (DDA) (Gao et al. 2016) is probably the most closest to our feature aggregation method as it also handles the bursts problem by diffusion. However, there exists at least a distinctive difference between our method and DDA. Specifically, we start from the heat equation, and balance the influence between rare features and frequent ones by enforcing the temperature of the system be a constant. While DDA inherited from Generalized Max-Pooling (GMP) (Murray et al. 2017), which equalized the contribution of a single descriptor to the aggregated vector.

## Deep Learning for Image Retrieval

Early attempts to use deep learning for image retrieval considered the use of the activations of fully connected layers as image-level descriptors (Babenko et al. 2014; Razavian et al. 2014; Gong et al. 2014). In (Babenko et al. 2014), a global representation was derived from the output of the penultimate layer. This work was among the first to show better performance than traditional methods based on SIFT-like features at the same dimensionality. Concurrently, Gong et al. (Gong et al. 2014) extracted multiple fully-connected activations by partitioning images into fragments, and then used VLAD-embeddings (Jégou et al. 2010) to aggregate the activations into a single image vector. The work (Razavian et al. 2014) reported promising results using sets of a few dozen features from the fully-connected layers of a CNN, without aggregating them into a global descriptor. However, observing that neural activations of the lower layers of a CNN capture more spatial details, later works advocated using the outputs of convolutional layers as features (Babenko and Lempitsky 2015; Kalantidis, Mellina, and Osindero 2016; Hoang et al. 2017; Tolias, Sicre, and Jégou 2016; Azizpour et al. 2015; Razavian et al. 2016; Xu et al. 2018). In our work, we follow this approach and use the outputs of the last convolutional layer of a pre-trained or fine-tuned convolutional neural network.

Considerable effort has been dedicated to aggregating the activations of convolutional layers into a distinctive global image vector. For instance, (Azizpour et al. 2015; Razavian et al. 2016) evaluated image-level descriptors obtained using max-pooling over the last convolutional layer, while Babenko and Lempitsky (Babenko and Lempitsky 2015) showed that sum-pooling leads to better performance. Kalantidis et al. (Kalantidis, Mellina, and Osindero 2016) further proposed a non-parametric method to learn weights for both spatial locations and feature channels. Related to that, Hoang et al. (Hoang et al. 2017) proposed several masking schemes to select a representative subset of local features before aggregation, and got satisfactory results by taking advantage of a triangulation embedding (Jégou and Zisserman 2014). In another work, Tolias et al. (Tolias, Sicre, and Jégou 2016) computed a collection of region vectors with max-pooling on the final convolutional layer, and then combined all region vectors into a final global representation. More recently, Xu et al. (Xu et al. 2018) independently employed selected part detectors to generate regional representations with weighted sum-pooling (Kalantidis, Mellina, and Osindero 2016), and then concatenated regional vectors as the global descriptor. In our work, we instead propose heat diffusion to weight and then aggregate deep feature descriptors.

Fine-tuning an off-the-shell network is also popular for performance improvement. For instance, there are a number of approaches that learn features for the specific task of landmark retrieval (Radenović, Tolias, and Chum 2016; Gordo et al. 2016; Arandjelovic et al. 2016; Cao et al. 2016). While fine-tuning a pre-trained model is usually preceded by extensive manual annotation, Radenovic et al. (Radenović, Tolias, and Chum 2016) introduced an unsupervised fine-tuning of CNN for image retrieval from a large collection of unordered images in a fully automated manner. Similar to (Radenović, Tolias, and Chum 2016), the works of (Arandjelovic et al. 2016; Cao et al. 2016) overcame laborious annotation, and collected training data in a weakly supervised manner. More specifically, Arandjelovic et al. (Arandjelovic et al. 2016) proposed a new network architecture, NetVLAD, that is trained for place recognition in an end-to-end manner from weakly supervised Google Street View Time Machine images. Cao et al. (Cao et al. 2016) trained a special architecture Quartet-net by harvesting data automatically from GeoPair (Thomee et al. 2016). We show that our feature selection, weighting, and re-ranking approach, while not requiring extra supervision, performs favorably compared to these previous methods.

In a couple of very recent works (Iscen et al. 2017a; 2017b), images were represented by multiple high-dimensional regional vectors. These two approaches achieve great performance on common benchmarks, they are however computationally demanding, both in terms of memory and computational usage. In contrast, our work uses a single vector representation while achieving similar performance.

## Feature Weighting with the Heat Equation

Given an input image  $I$  that is fed through a pre-trained or a fine-tuned CNN, the activations (responses) of a convolutional layer form a 3D tensor  $\mathbf{X} \in \mathbb{R}^{W \times H \times K}$ , where

$W \times H$  is the spatial resolution of the feature maps, and  $K$  is the number of feature maps (channels). We denote  $\mathcal{V} = \{\mathbf{f}_m\}$  as a set of  $W \times H$  local features, where  $\mathbf{f}_m$  is a  $K$ -dimensional vector at spatial location  $(i, j)$  in  $\mathbf{X}$ . That is to say,  $m = i + (j - 1) \times W$ , where  $1 \leq i \leq W$  and  $1 \leq j \leq H$ . We assume that Rectified Linear Units (ReLU) are applied as a last step, guaranteeing that all elements of  $\mathbf{f}_m$  are non-negative.

### Problem Formulation

We utilize the theory of anisotropic diffusion (Weickert 1998) to compute weights for each feature in  $\mathcal{V}$  based on their distinctiveness, thus avoiding the burstiness issue. Let  $\mathcal{G} = (\mathcal{V}, \mathcal{E})$  denote an undirected graph, where  $\mathcal{V}$  is the set of nodes, and  $\mathcal{E} = \{e(\mathbf{f}_m, \mathbf{f}_n), \forall (\mathbf{f}_m, \mathbf{f}_n) \in \mathcal{V}^2\}$  is the set of edges. By assigning  $\mathbf{f}_l$  as the heat source, we assume that the graph constitutes a heat transfer system where  $\mu_l(m, t)$  is the temperature at node  $\mathbf{f}_m$  at time  $t$ , and  $\mathbf{P}$  is a  $|\mathcal{V}| \times |\mathcal{V}|$  positive definite symmetric matrix called the *diffusion tensor*. Then the *heat equation* for this system is defined as follows:

$$\partial_t \boldsymbol{\mu} = \text{div}(\mathbf{P} \nabla \boldsymbol{\mu}) \quad (1)$$

Our problem is to compute the temperature at each node  $\mathbf{f}_m$ . That is,

$$\begin{cases} \frac{\partial \mu_l(m, t)}{\partial t} = \text{div}(\mathbf{P} \nabla \mu_l(m, t)), \\ \text{s.t. } \mu_l(g) = 0, \mu_l(l) = 1, \end{cases} \quad (2)$$

where we use *Dirichlet* boundary conditions (Weickert 1998), and assume that the temperature of the environment node (outside of the system) and the source node is always zero (i.e.,  $\mu_l(g) = 0$ ) and one (i.e.,  $\mu_l(l) = 1$ ), respectively.

In practice, we compute the temperature at each node with the following simplified assumptions. Specifically, we let  $t \rightarrow +\infty$  and consequently drop  $t$  in our method as we are interested in the steady state, and define the diffusion tensor  $\mathbf{P}$  by the *cosine* similarity between feature vectors:

$$P(m, n) = \begin{cases} 0, & m = n, \\ \frac{\mathbf{f}_m^T \mathbf{f}_n}{\|\mathbf{f}_m\| \|\mathbf{f}_n\|}, & m \neq n. \end{cases} \quad (3)$$

Furthermore, we assume that the dissipation heat loss at a node  $\mathbf{f}_m$  is  $\lambda_m$ , which is constant in time. In other words, each node  $\mathbf{f}_m \in \mathcal{V} \setminus \mathbf{f}_l$  is connected to an environment node  $g$  with diffusivity of  $\lambda_m$ . With these assumptions, the heat diffusion Eq.(2) reduces to the simplified version (Weickert 1998; Grady 2006):

$$\begin{cases} \mu_l(m) = \frac{1}{a_m} \sum P(m, n) \mu_l(n), \\ \text{s.t. } \mu_l(g) = 0, \mu_l(l) = 1, \end{cases} \quad (4)$$

where  $a_m = \sum P(m, n) + \lambda_m$ ,  $m \neq g, l$ . Without loss of generality, we assume  $\mathbf{P} = (0, \mathbf{P}_1^T; \mathbf{P}_1, \mathbf{P}_2)$ , where  $\mathbf{P}_1 \in \mathbb{R}^{(|\mathcal{V}|-1) \times 1}$  stores the similarities between points in  $\mathcal{V} \setminus \mathbf{f}_l$  and  $\mathbf{f}_l$ , and  $\mathbf{P}_2 \in \mathbb{R}^{(|\mathcal{V}|-1) \times (|\mathcal{V}|-1)}$  stores the similarities between any two pair points in  $\mathcal{V} \setminus \mathbf{f}_l$ . Then, Eq.(4) can be rewritten as

$$\boldsymbol{\mu}_l = (\mathbf{I}_{|\mathcal{V}|-1} - \boldsymbol{\Lambda}_l^{-1} \mathbf{P}_2)^{-1} (\boldsymbol{\Lambda}_l^{-1} \mathbf{P}_1), \quad (5)$$

where  $\mathbf{I}_{|\mathcal{V}|-1}$  is the identity matrix of size  $(|\mathcal{V}|-1) \times (|\mathcal{V}|-1)$ , and  $\boldsymbol{\Lambda}_l = \text{diag}(a_1, \dots, a_{l-1}, a_{l+1}, \dots, a_{|\mathcal{V}|})$  is the diagonal matrix. Thus, the temperature of the system is

$$\psi_l = \sum_{m=1}^{|\mathcal{V}|} \mu_l(m). \quad (6)$$

We greedily consider each point  $\mathbf{f}_l \in \mathcal{V}$  as a heat source, and compute the system temperature  $\psi_l$  of all the other points under the linear anisotropic diffusion equation. The value of  $\psi_l$  can indicate whether  $\mathbf{f}_l$  is a frequent feature or a rare one. Intuitively, a *bursty* feature is densely connected to other features with high similarities, which consequently rises the temperature of the system. In contrast, a rare feature connects other features sparsely and therefore causes the system temperature to be low. Thus, in order to balance the influence between rare features and frequent ones, we enforce the temperature of the system be a constant by introducing a set of weighting coefficients  $w_l$ . That is,

$$w_l \times \psi_l = 1, \forall \mathbf{f}_l \in \mathcal{V}. \quad (7)$$

As a result,  $w_l$  is used to reduce the burstiness effects, and we accordingly compute the final image representation  $\mathbf{v}_I$  of each image  $I$  by

$$\mathbf{v}_I = \frac{\left( \sum_{l=1}^{|\mathcal{V}|} w_l \mathbf{f}_l \right)^\alpha}{\left\| \left( \sum_{l=1}^{|\mathcal{V}|} w_l \mathbf{f}_l \right)^\alpha \right\|}, \quad (8)$$

where  $0 < \alpha \leq 1$  is a constant, and we typically set  $\alpha = 0.5$ .  $\alpha$  plays the same role as the exponent parameter in the Power-law Normalization (PN) formula (Perronnin, Sánchez, and Mensink 2010). However, it is worth noting that, we apply  $\alpha$ -normalisation on the image vector *before* PCA whitening, while PN is integrated in the retrieval frameworks (Murray et al. 2017; Do and Cheung 2017) *after* rotating the image representation with a PCA rotation matrix. Fig. 1 visualizes the weights computed for two sample input images, larger weights are shown in warmer colors. As shown, our feature weighting method assigns larger weights to distinctive areas, and smaller weights to repetitive ones.

For convenience, in the following we denote our heat equation based feature weighting method presented in this section as HeW.

### Computing Weights in Practice

It seems that we have to solve Eq.(5)  $|\mathcal{V}|$  times to get the image representation of  $I$ , and each time we need to solve a linear equation of size  $(|\mathcal{V}|-1) \times (|\mathcal{V}|-1)$ . Thus, the total time cost of HeW is about in  $O(|\mathcal{V}|^4)$ . This might be computationally intensive if the selected feature set cardinality  $|\mathcal{V}|$  is large.

However, the actual time complexity can be reduced to  $O(|\mathcal{V}|^3)$ , and we can compute all  $\psi_l$  by inverting the matrix  $(\mathbf{I}_{|\mathcal{V}|} - \boldsymbol{\Lambda}^{-1} \mathbf{P})$  only once, where  $\boldsymbol{\Lambda} = \text{diag}(a_1, \dots, a_{|\mathcal{V}|})$ . Specifically, we take computing  $\psi_1$  as an example to illustrate the practical computational process. We leverage the block structure of  $(\mathbf{I}_{|\mathcal{V}|} - \boldsymbol{\Lambda}^{-1} \mathbf{P})$ , i.e.,

$$\mathbf{I}_{|\mathcal{V}|} - \boldsymbol{\Lambda}^{-1} \mathbf{P} = \begin{bmatrix} 1 & -\mathbf{x}^T \\ -\mathbf{y} & \mathbf{Q} \end{bmatrix}, \quad (9)$$

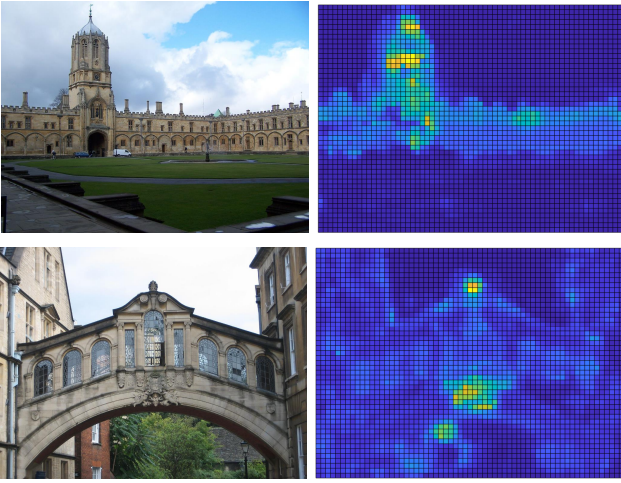


Figure 1: Two example visualization results of the proposed method with deep features extracted using the SiaMAC $\dagger$  (Radenović, Tolias, and Chum 2016) CNN model. Left: the original image; Right: relative weights (warmer colors indicate larger weights) for selected features. For instance, in the top image, there seems to be distinctive areas at the locations of the tower.

where  $\mathbf{x}$  and  $\mathbf{y}$  are vectors of size  $|\mathcal{V}|-1$ , and  $\mathbf{Q}$  is the matrix of size  $(|\mathcal{V}|-1) \times (|\mathcal{V}|-1)$ . According to Eqs. (5) and (6), it is easy to know that

$$\psi_1 = \sum \mathbf{Q}^{-1} \mathbf{y} + 1. \quad (10)$$

By leveraging the property of the block matrix, we can derive that  $(\mathbf{I}_{|\mathcal{V}|} - \mathbf{\Lambda}^{-1} \mathbf{P})^{-1} =$

$$\begin{bmatrix} 1 + \mathbf{x}^T (\mathbf{Q} - \mathbf{y} \mathbf{x}^T)^{-1} \mathbf{y} & \mathbf{x}^T (\mathbf{Q} - \mathbf{y} \mathbf{x}^T)^{-1} \\ (\mathbf{Q} - \mathbf{y} \mathbf{x}^T)^{-1} \mathbf{y} & (\mathbf{Q} - \mathbf{y} \mathbf{x}^T)^{-1} \end{bmatrix}. \quad (11)$$

Furthermore, one can prove that

$$\mathbf{Q}^{-1} \mathbf{y} = \frac{(\mathbf{Q} - \mathbf{y} \mathbf{x}^T)^{-1} \mathbf{y}}{1 + \mathbf{x}^T (\mathbf{Q} - \mathbf{y} \mathbf{x}^T)^{-1} \mathbf{y}}. \quad (12)$$

The above three equations demonstrate that we can derive  $\psi_1$  by using the first column of  $(\mathbf{I}_{|\mathcal{V}|} - \mathbf{\Lambda}^{-1} \mathbf{P})^{-1}$ . Similarly, we can get  $\psi_l$  using the  $l$ -th column of  $(\mathbf{I}_{|\mathcal{V}|} - \mathbf{\Lambda}^{-1} \mathbf{P})^{-1}$ :

$$\psi_l = \frac{\sum_{m=1, m \neq l}^{|\mathcal{V}|} (\mathbf{I}_{|\mathcal{V}|} - \mathbf{\Lambda}^{-1} \mathbf{P})^{-1}(m, l)}{(\mathbf{I}_{|\mathcal{V}|} - \mathbf{\Lambda}^{-1} \mathbf{P})^{-1}(l, l)} + 1. \quad (13)$$

Thus, the conclusion that the computational cost is in  $O(|\mathcal{V}|^3)$  holds.

## Experiments and Results

This section describes the implementation of our method, and reports results on public image retrieval benchmarks. Throughout the section, we normalize the final image vector to have unit Euclidean norm.

## Datasets and Evaluation Protocol

We evaluate our method on three public datasets: **Oxford Buildings** (Oxford5k) (Philbin et al. 2007), **Paris** (Paris6k) (Philbin et al. 2008), and **INRIA Holidays** (Holidays) (Jégou, Douze, and Schmid 2010).

**Oxford5k** contains a set of 5,062 photographs comprising 11 different Oxford landmarks. There are 55 query images with each 5 queries corresponding to a landmark. Following the standard protocol, we crop the query images based on the provided bounding boxes before retrieval. The performance is measured using mean average precision (mAP) over the 55 queries, where *junk* images are removed from the ranking.

**Paris6k** consists of 6,392 high resolution images of the city Paris. This dataset also provides 55 query images and their corresponding ground truth relevant images. We also use cropped query images to perform retrieval, and measure the overall retrieval performance using mAP.

**Holidays** includes 1,491 images in total, and selects 500 images as queries associated with the 500 partitioning groups of the image set. To be directly comparable with recent works (Babenko and Lempitsky 2015; Kalantidis, Mellina, and Osindero 2016; Hoang et al. 2017), we manually fix images in the wrong orientation by rotating them by  $\pm 90$  degrees. The retrieval quality is also measured using mAP over 500 queries, with the query removed from the ranked list.

**Flickr100k** (Philbin et al. 2007) was crawled from Flickr’s 145 most popular tags and consists of 11,071 images. We combine these 100k distractor images with Oxford5k and Paris6k, and produce Oxford105k and Paris106k datasets respectively. In this way, we evaluate the behavior of our method at a larger scale.

## Implementation Notes

**Deep convolutional features.** In order to extensively evaluate our method, we use a pre-trained and a fine-tuned deep neural networks to extract multiple convolutional features for each image. The adopted pre-trained network is VGG16 (Simonyan and Zisserman 2014), which is widely used in the literature. The fine-tuned network is siaMAC $\dagger$  (Radenović, Tolias, and Chum 2016), a popular fine-tuned model of VGG16.

Following the practice of previous works (Kalantidis, Mellina, and Osindero 2016; Radenović, Tolias, and Chum 2016), we choose the last convolutional layer of each network to separately extract patch-level image features. We use public available trained models. Specifically, we use the Matconvnet toolbox (Vedaldi and Lenc 2015) for VGG16, and use the model provided in (Arandjelovic et al. 2016) for siaMAC $\dagger$ . In addition, in order to accelerate feature extraction, we resize the longest side of all images to 1,024 pixels while preserving aspect ratios before using them as input to each deep network.

**PCA whitening** is widely used in many image retrieval systems (Jégou and Chum 2012; Kalantidis, Mellina, and Osindero 2016; Hoang et al. 2017; Babenko and Lempitsky 2015) as it can effectively improve the discriminative ability of image vectors. In order to avoid over-fitting, the

Table 1: Efficiency comparisons for considered combinations on Oxford105k. We measure image representation time with images of size  $1,024 \times 768$  (the number of features is typically 3,072). For image representation time, we do not include time for feature extraction.

Method	Representation time	Query time with varied representation dimensions				
		32	64	128	256	512
SumA	13ms	8ms	9ms	11ms	13ms	15ms
HeW	173ms	14ms	15ms	16ms	17ms	19ms
SumA+QE	13ms					
HeW+QE	173ms					

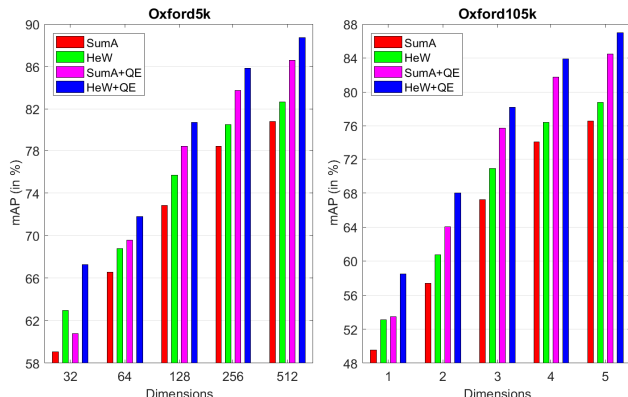


Figure 2: Comparison results of HeW and SumA without and with re-ranking by varying dimensions of image vectors. Short representations are achieved by keeping only the first components of 512 dimensional image vectors after PCA whitening.

PCA matrix is usually learned with the set of aggregated image vectors produced from a held-out dataset. To be directly comparable with related works, we learn PCA parameters on Paris6k for Oxford5k and Oxford105k, and on Oxford5k for Paris6k and Paris106k. As for Holidays, we randomly select a subset of 5000 images from Flickr100k to learn parameters.

**Query Expansion (QE)** (Chum et al. 2007) is an effective post-processing technique to increase retrieval performance. Given the ranked list of database images over a query image, we simply calculate the average vector of the 10 top-ranked image vectors and the query vector, and we then use the  $L_2$  normalized average vector to re-query again.

## Preliminary Experiments

We evaluate the retrieval performance of our method for different settings with deep convolutional features extracted by siaMAC<sup>†</sup> on Oxford5k and Oxford105k. Specifically, we evaluate the following four combinations: SumA, HeW, SumA+QE and HeW+QE. SumA means we obtain image representations by simply summing all the features of each image, and perform image search by linearly scanning database vectors. It justifies the contribution of our deep feature aggregation method HeW, therefore it can be considered as our baseline. SumA+QE and HeW+QE indicate that we perform re-ranking QE with image vectors produced by

SumA and HeW, respectively. They are used to further compare SumA and HeW after re-ranking.

**Performance comparison.** We illustrate mAP curves when varying the dimensionality of the final image vectors from 32 to 512 in Fig.2. Dimensionality reduction is achieved by keeping only the first  $D$  components of 512 dimensional image vectors after PCA whitening. As we see, the gain of HeW over SumA is about 2% in mAP on both Oxford5k and Oxford105k at  $D = 512$ . Furthermore, the performance gain is increasing with the reduction of the number of dimensions, and the gain is about 4% at  $D = 32$ . After incorporating QE, the performance advantage is enlarged, and the increased mAP value of HeW over SumA on both datasets is more than 5% at  $D = 32$ .

**Efficiency comparison.** Table 1 reports timings (excluding time for feature extraction) measured to compute image representations and to perform image querying. We implement both SumA and HeW in Matlab, and benchmarks are obtained on an Intel Xeon E5-2630/2.20GHz with 20 cores. As the table shows, although the baseline method SumA is faster than HeW by about an order of magnitude, HeW is still fast in practice. For an image of high resolution  $1,024 \times 768$ , the number of deep features is 3,072, and the time to derive image vector with HeW is typically 173ms. Furthermore, it is easy to know that HeW does not affect search efficiency, and it has the same searching time as SumA. Thus, the online query time for HeW is about 188ms at  $D = 512$ .

The increased time caused by incorporating image re-ranking into the retrieval system is limited. As shown, the total online processing time for HeW+QE with  $D = 512$  is only about 192ms. This means searching with our method is efficient in practice.

## Comparison with the State-of-the-art

**Comparison with methods using SIFT and pre-trained networks.** In Table 2, we present comparisons of our approach using VGG16 with methods using SIFT and off-the-shell available networks, which utilize global representations of images. The comparison results are summarized as follows:

- Our approach significantly outperforms two state-of-the-art methods (Do and Cheung 2017; Murray et al. 2017) using weaker SIFT features, although their dimensions are more than 10 times higher than ours. Furthermore, it also shows clear advantages over (Gong et al. 2014; Babenko et al. 2014; Razavian et al. 2014) that utilize

Table 2: Performance (in mAP) comparison with methods using SIFT and off-the-shell available networks. As many previous works (Kalantidis, Mellina, and Osindero 2016; Radenović, Tolias, and Chum 2016), we do not perform query expansion on Holidays as each query only has a few ground truth similar images.

Feature	Method	Dim.	Ox5k	Ox105k	Pa6k	Pa106k	Holidays
SIFT	F-FAemb (Do and Cheung 2017)	7,245	66.1	64.3	–	–	75.5
	Temb (Murray et al. 2017)	8,064	70.0	64.4	–	–	71.6
Fully connected layer	MOP-CNN (Gong et al. 2014)	2,048	–	–	–	–	80.8
	Neural codes (Babenko et al. 2014)	4,096	54.5	51.2	–	–	79.3
	CNNaug-ss (Razavian et al. 2014)	4,096	68.0	–	79.5	–	84.3
Conv. layer of VGG16	R-MAC (Tolias, Sicre, and Jégou 2016)	512	66.9	61.6	<b>83.0</b>	75.7	–
	CroW (Kalantidis, Mellina, and Osindero 2016)	512	70.8	65.3	79.7	72.2	85.1
	MAX-mask (Hoang et al. 2017)	512	65.7	60.5	81.6	72.4	85.0
	PWA (Xu et al. 2018)	512	72.0	66.2	82.3	<b>75.8</b>	–
	HeW	512	<b>72.8</b>	<b>68.0</b>	81.5	74.4	<b>88.4</b>
	R-MAC+AML+QE (Tolias, Sicre, and Jégou 2016)	512	77.3	73.2	86.5	79.8	–
	CroW+QE (Kalantidis, Mellina, and Osindero 2016)	512	74.9	70.6	84.8	79.4	–
	PWA+QE (Xu et al. 2018)	512	74.8	72.5	86.0	80.7	–
	HeW+QE	512	<b>77.4</b>	<b>74.9</b>	<b>87.0</b>	<b>82.7</b>	–

Table 3: Performance (in mAP) comparison with the state-of-the-art methods using unsupervised fine-tuned networks.

Method	Dim.	Ox5k	Ox105k	Pa6k	Pa106k	Holidays
NetVLAD (Arandjelovic et al. 2016)	512	67.6	–	74.9	–	86.1
siaMAC†+MAC (Radenović, Tolias, and Chum 2016)	512	79.0	73.9	82.4	74.6	79.5
siaMAC†+R-MAC (Radenović, Tolias, and Chum 2016)	512	77.0	69.2	83.8	76.4	82.5
siaMAC†+MAX-mask (Hoang et al. 2017)	512	77.7	72.7	83.2	76.5	86.3
Fisher Vector (Ong, Husain, and Bober 2017)	512	81.5	76.6	82.4	–	–
siaMAC†+HeW	512	<b>82.6</b>	<b>78.8</b>	<b>86.9</b>	<b>81.2</b>	<b>87.1</b>
siaMAC†+MAC (Radenović, Tolias, and Chum 2016)	256	77.4	70.7	80.8	72.2	77.3
siaMAC†+R-MAC (Radenović, Tolias, and Chum 2016)	256	74.9	67.5	82.3	74.1	81.4
siaMAC†+HeW	256	<b>80.5</b>	<b>76.5</b>	<b>85.2</b>	<b>79.5</b>	<b>85.9</b>
siaMAC†+MAC (Radenović, Tolias, and Chum 2016)	128	75.8	68.6	77.6	68.0	73.2
siaMAC†+R-MAC (Radenović, Tolias, and Chum 2016)	128	72.5	64.3	78.5	69.3	79.3
siaMAC†+HeW	128	<b>75.7</b>	<b>70.9</b>	80.8	74.1	<b>85.0</b>
siaMAC†+MAC+R+QE (Radenović, Tolias, and Chum 2016)	512	85.0	81.8	86.5	78.8	–
siaMAC†+R-MAC+R+QE (Radenović, Tolias, and Chum 2016)	512	82.9	77.9	85.6	78.3	–
siaMAC†+HeW+QE	512	<b>88.7</b>	<b>86.9</b>	<b>90.5</b>	<b>86.4</b>	–
siaMAC†+HeW+QE	256	85.8	83.9	89.5	85.3	–
siaMAC†+HeW+QE	128	80.7	78.2	85.8	80.1	–

fully connected layers to derive image representations.

- Compared with (Tolias, Sicre, and Jégou 2016; Kalantidis, Mellina, and Osindero 2016; Hoang et al. 2017; Xu et al. 2018) which are also using the VGG16 model, our method achieves the best results on Oxford5k, Oxford105k and Holidays. Additionally, it is worth noting that, the gain on Holidays is over 3% at the same dimensionality.
- When combined with query expansion, our approach produces the best results on the four considered datasets. As shown, the gains over compared methods on two large-scale datasets Oxford105k and Paris106k are at least 1.7% and 2.0%, respectively.

#### Comparison with methods using fine-tuned networks.

We perform comparisons with recent unsupervised fine-tuned methods (Arandjelovic et al. 2016; Radenović, Tolias, and Chum 2016; Hoang et al. 2017; Ong, Husain, and Bober 2017) in Table 3. The table again demonstrates the superior

performance of our approach over related baselines at the same dimensionality:

- We establish new state-of-the-art results on all evaluated datasets at dimensionality of 512, and the improved mAP values are not negligible. For example, the gain on Paris106k is at least 4.7%.
- With the same siaMAC† features, our approach improves two related baselines R-MAC and MAC presented in (Radenović, Tolias, and Chum 2016) without and with dimensionality reduction, and the improvement is more significant on two large datasets: Oxford105k and Paris106k.
- Our method, HeW, also produces much better results than (Radenović, Tolias, and Chum 2016) after query expansion, although (Radenović, Tolias, and Chum 2016) uses more sophisticated post-processing than us. Additionally, HeW outperforms the best competing method at  $D = 256$ , and keeps competitive even at  $D = 128$ .

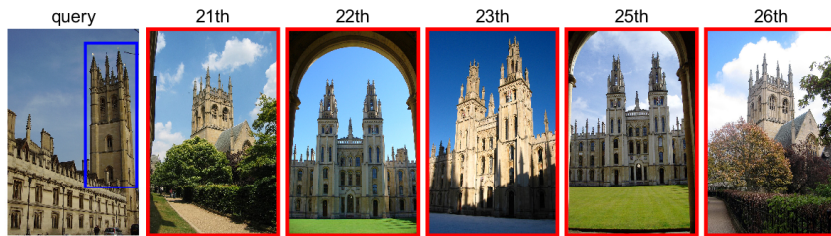


Figure 3: A query image from Oxford105k and its top five false positive results returned by our approach HeW+QE. We consider it is a failure case for our method as its average precision is only 54.3%.

Table 4: Comparison with the best results reported in the literature.

Method	Dim.	Oxford5k	Oxford105k	Paris6k	Paris106k	Holidays
Mikulik et al. (Mikulik et al. 2013)	16M	84.9	82.4	79.5	77.3	75.8
Tolias et al. (Tolias, Avrithis, and Jégou 2013)	8M	87.9	–	85.4	–	85.0
Tolias and Jégou (Tolias and Jégou 2015)	8M	89.4	84.0	82.8	–	–
Arandjelovic et al. (Arandjelovic et al. 2016)	4,096	71.6	–	79.7	–	87.5
Hoang et al. (Hoang et al. 2017)	4,096	83.8	80.6	88.3	83.1	<b>92.2</b>
Ischen et al. (Ischen et al. 2017a)	5×512	91.5	84.7	<b>95.6</b>	<b>93.0</b>	–
Ischen et al. (Ischen et al. 2017b)	5×512	<b>91.6</b>	86.5	95.6	92.4	–
This paper	512	88.7	<b>86.9</b>	90.5	86.4	88.4

To better understand our method HeW+QE, we visualize the top five false positive images for a query image from Oxford105k in Fig. 3. This query can be considered as a failure case for our method as its average precision is only 54.3%, falling far behind the mAP value of 86.9%. As displayed, although landmarks contained in the 21-th and 26-th images are exactly not the same as the one contained in the query, they are visually similar to the query.

**Comparison with costly methods.** Table 4 compares our best results with the very best results obtained in the literature. Some of them (Ischen et al. 2017a; 2017b) do not necessarily rely on a global representation, and some others (Mikulik et al. 2013; Tolias, Avrithis, and Jégou 2013; Arandjelovic et al. 2016; 2016; Hoang et al. 2017) represent images with much higher dimensional vectors, and are thus not directly comparable. There is no doubt that these methods use a larger memory footprint and searching time than our approach.

## Conclusions

We proposed an aggregation approach for building compact but powerful image representations by utilizing the heat equation. By considering each feature as a heat source, our approach avoided over-representation of bursty features by enforcing the temperature of the system be a constant. We provided a practical solution to derive image vectors, and demonstrated the effectiveness of our method on the task of instance-level retrieval. Our method is unsupervised, and can be compatible with different CNNs, including pre-trained and fine-tuned networks. Experimental results showed that we establish new state-of-the-art results on public image retrieval benchmarks using 512-dimensional vector representations.

## Acknowledgments

This work was supported by National Key Research and Development Plan 2016YFB1001004, National Natural Science Foundation of China Grant 61603289, China Postdoctoral Science Foundation Grant 2016M602823, and Fundamental Research Funds for the Central Universities xjj2017118. This work was done when the first author was a visiting scholar at University of Virginia.

## References

- Arandjelovic, R.; Gronat, P.; Torii, A.; Pajdla, T.; and Sivic, J. 2016. NetVLAD: CNN architecture for weakly supervised place recognition. In *CVPR*, 5297–5307.
- Azizpour, H.; Razavian, A. S.; Sullivan, J.; Maki, A.; and Carlsson, S. 2015. From generic to specific deep representations for visual recognition. In *CVPR DeepVision Workshop*, 36–45.
- Babenko, A., and Lempitsky, V. 2015. Aggregating local deep features for image retrieval. In *ICCV*, 1269–1277.
- Babenko, A.; Slesarev, A.; Chigorin, A.; and Lempitsky, V. 2014. Neural codes for image retrieval. In *ECCV*, 584–599.
- Bruhn, A.; Weickert, J.; and Schnörr, C. 2005. Lucas/kanade meets horn/schunck: Combining local and global optic flow methods. *IJCV* 61(3):211–231.
- Cao, J.; Huang, Z.; Wang, P.; Li, C.; Sun, X.; and Shen, H. T. 2016. Quartet-net learning for visual instance retrieval. In *ACM MM*, 456–460.
- Chum, O.; Philbin, J.; Sivic, J.; Isard, M.; and Zisserman, A. 2007. Total recall: Automatic query expansion with a generative feature model for object retrieval. In *ICCV*, 1–8.

- Do, T.-T., and Cheung, N.-M. 2017. Embedding based on function approximation for large scale image search. *IEEE TPAMI* 99:1–12.
- Donoser, M., and Bischof, H. 2013. Diffusion processes for retrieval revisited. In *CVPR*, 1320–1327.
- Egozi, A.; Keller, Y.; and Guterman, H. 2010. Improving shape retrieval by spectral matching and meta similarity. *IEEE TIP* 19(5):1319–1327.
- Furuya, T., and Ohbuchi, R. 2015. Diffusion-on-manifold aggregation of local features for shape-based 3d model retrieval. In *ICMR*, 171–178.
- Gao, Z.; Xue, J.; Zhou, W.; Pang, S.; and Tian, Q. 2016. Democratic diffusion aggregation for image retrieval. *IEEE TMM* 18(8):1661–1674.
- Gong, Y.; Wang, L.; Guo, R.; and Lazebnik, S. 2014. Multi-scale orderless pooling of deep convolutional activation features. In *ECCV*, 392–407.
- Gordo, A.; Almazán, J.; Revaud, J.; and Larlus, D. 2016. Deep image retrieval: Learning global representations for image search. In *ECCV*, 241–257.
- Grady, L. 2006. Random walks for image segmentation. *IEEE TPAMI* 28(11):1768–1783.
- Hoang, T.; Do, T.-T.; Tan, D.-K. L.; and Cheung, N.-M. 2017. Selective deep convolutional features for image retrieval. In *ACM MM*, 1600–1608.
- Iscen, A.; Tolias, G.; Avrithis, Y.; Furon, T.; and Chum, O. 2017a. Efficient diffusion on region manifolds: Recovering small objects with compact CNN representations. In *CVPR*, 926–935.
- Iscen, A.; Tolias, G.; Avrithis, Y.; Furon, T.; and Chum, O. 2017b. Fast spectral ranking for similarity search. *arXiv preprint arXiv:1703.06935*.
- Jégou, H., and Chum, O. 2012. Negative evidences and co-occurrences in image retrieval: The benefit of PCA and whitening. In *ECCV*, 774–787.
- Jégou, H., and Zisserman, A. 2014. Triangulation embedding and democratic aggregation for image search. In *CVPR*, 3310–3317.
- Jégou, H.; Douze, M.; Schmid, C.; and Pérez, P. 2010. Aggregating local descriptors into a compact image representation. In *CVPR*, 3304–3311.
- Jégou, H.; Douze, M.; and Schmid, C. 2009. On the burstiness of visual elements. In *CVPR*, 1169–1176.
- Jégou, H.; Douze, M.; and Schmid, C. 2010. Improving bag-of-features for large scale image search. *IJCV* 87(3):316–336.
- Kalantidis, Y.; Mellina, C.; and Osindero, S. 2016. Cross-dimensional weighting for aggregated deep convolutional features. In *ECCV Workshops*, 685–701.
- Kim, G.; Xing, E. P.; Fei-Fei, L.; and Kanade, T. 2011. Distributed cosegmentation via submodular optimization on anisotropic diffusion. In *ICCV*, 169–176.
- Mikulik, A.; Perdoch, M.; Chum, O.; and Matas, J. 2013. Learning vocabularies over a fine quantization. *IJCV* 103(1):163–175.
- Murray, N.; Jégou, H.; Perronnin, F.; and Zisserman, A. 2017. Interferences in match kernels. *IEEE TPAMI* 39(9):1797–1810.
- Ong, E.-J.; Husain, S.; and Bober, M. 2017. Siamese network of deep fisher-vector descriptors for image retrieval. *arXiv preprint arXiv:1702.00338*.
- Perona, P., and Malik, J. 1990. Scale-space and edge detection using anisotropic diffusion. *IEEE TPAMI* 12(7):629–639.
- Perronnin, F.; Sánchez, J.; and Mensink, T. 2010. Improving the fisher kernel for large-scale image classification. In *ECCV*, 143–156.
- Philbin, J.; Chum, O.; Isard, M.; Sivic, J.; and Zisserman, A. 2007. Object retrieval with large vocabularies and fast spatial matching. In *CVPR*, 1–8.
- Philbin, J.; Chum, O.; Isard, M.; Sivic, J.; and Zisserman, A. 2008. Lost in quantization: Improving particular object retrieval in large scale image databases. In *CVPR*, 1–8.
- Radenović, F.; Tolia, G.; and Chum, O. 2016. CNN image retrieval learns from BoW: Unsupervised fine-tuning with hard examples. In *ECCV*, 3–20.
- Razavian, A. S.; Azizpour, H.; Sullivan, J.; and Carlsson, S. 2014. CNN features off-the-shelf: an astounding baseline for recognition. In *CVPR Workshops*, 512–519.
- Razavian, A. S.; Sullivan, J.; Carlsson, S.; and Maki, A. 2016. Visual instance retrieval with deep convolutional networks. *ITE TMTA* 4(3):251–258.
- Simonyan, K., and Zisserman, A. 2014. Very deep convolutional networks for large-scale image recognition. *arXiv preprint arXiv:1409.1556*.
- Thomee, B.; Shamma, D. A.; Friedland, G.; Elizalde, B.; Ni, K.; Poland, D.; Borth, D.; and Li, L.-J. 2016. YFCC100M: the new data in multimedia research. *Communications of the ACM* 59(2):64–73.
- Tolias, G., and Jégou, H. 2015. Visual query expansion with or without geometry: Refining local descriptors by feature aggregation. *Pattern Recognition* 47(10):3466–3476.
- Tolias, G.; Avrithis, Y.; and Jégou, H. 2013. To aggregate or not to aggregate: Selective match kernels for image search. In *ICCV*, 1401–1408.
- Tolias, G.; Sicre, R.; and Jégou, H. 2016. Particular object retrieval with integral max-pooling of CNN activations. In *ICLR*, 1–12.
- Tschumperle, D., and Deriche, R. 2005. Vector-valued image regularization with PDEs: A common framework for different applications. *IEEE TPAMI* 27(4):506–517.
- Vedaldi, A., and Lenc, K. 2015. Matconvnet: Convolutional neural networks for MATLAB. In *ACM MM*, 689–692.
- Weickert, J. 1998. *Anisotropic diffusion in image processing*. Teubner Stuttgart.
- Xu, J.; Shi, C.; Qi, C.; Wang, C.; and Xiao, B. 2018. Unsupervised partbased weighting aggregation of deep convolutional features for image retrieval. In *AAAI*, 1–8.
- Yang, X.; Koknar-Tezel, S.; and Latecki, L. J. 2009. Locally constrained diffusion process on locally densified distance

spaces with applications to shape retrieval. In *CVPR*, 357–364.

Zhang, J.; Zheng, J.; and Cai, J. 2010. A diffusion approach to seeded image segmentation. In *CVPR*, 2125–2132.